Materials Performance and Characterization

doi:10.1520/MPC20130038 / Vol. 3 / No. 2 / 2014 / available online at www.astm.org

Scott G. Keller[1] and Ali P. Gordon[2]

Coupled Fatigue Crack Initiation and Propagation Model Utilizing a Single Blunt Notch Compact Tension Specimen

Reference

Keller, Scott G. and Gordon, Ali P., "Coupled Fatigue Crack Initiation and Propagation Model Utilizing a Single Blunt Notch Compact Tension Specimen," *Materials Performance and Characterization*, Vol. 3, No. 2, 2014, pp. 110–136, doi:10.1520/MPC20130038.
ISSN 2165-3992

Manuscript received August 30, 2013; accepted for publication January 20, 2014; published online February 28, 2014.

[1] Mechanics of Materials Research Group, Univ. of Central Florida, 4000 Central Florida Blvd., Orlando, FL 32816, United States of America.

[2] Associate Professor, Mechanical and Aerospace Engineering Dept., Univ. of Central Florida, 4000 Central Florida Blvd., Orlando, FL 32816, United States of America.

ABSTRACT

Many power generation facilities equipped with turbomachinery are designed to provide electric energy on an as-needed basis and, as a consequence, impart a mixture of fatigue and creep damage to high-value components at elevated temperatures. Cracks are often initiated on free surfaces of these parts near stress-raising features and propagate under thermal-mechanical cycling until the component is removed from service. Whether the emphasis is on creep or fatigue failure, most conventional structural life prediction approaches decouple crack initiation from crack propagation. Turbine designers are in need of approaches that span the full life cycle of components in which both initiation and propagation are the consequences of a variety of mechanical failure modes. Although recent fracture mechanics methods have been developed to account for fatigue- and creep-crack growth, a tacit assumption is that a precrack exists. Another main limitation of these approaches is the small scale yielding assumption, associated with linear elastic fracture mechanics, in which extensive plasticity invalidates such analyses. In this study, utilizing a blunt notch compact tensile specimen, experimental routines involving crack initiation and propagation within a single specimen at elevated temperatures with plastic-inducing loads and hold periods were conducted. Founded on existing elastic and elastic-plastic

fracture mechanics (EPFM), a coupled crack initiation and propagation model is presented. Through the use of the EPFM parameter *J*, the proposed models are observed to accurately predict crack initiation and replicate crack propagation rates based on the imposed experimental conditions. The model is demonstrated on an austenitic stainless steel, type 304, subjected to moderate temperatures in air. Mechanical testing, metallurgical analysis, and analytical modeling allow for a simplified phenomenological life prediction model capable of predicting crack initiation and propagation at elevated temperatures. Consequently, structural analysis of critical locations of components can span the gamut of crack initiation, crack growth, and instability (i.e., total life assessment).

Keywords

fatigue crack initiation, fatigue crack growth, cyclic *J*-integral, elevated temperature testing

Introduction

Traditionally, the linear elastic fracture mechanics (LEFM) crack tip stress field parameter *K*, or the stress intensity factor, is utilized in fatigue crack growth analyses. The use of such a stress-modifying parameter in the analysis of fatigue crack propagation studies has been popular since correlations between the cyclic stress intensity range ΔK and crack growth rates were first made in the late 1950s [1]. The groundbreaking research provided the framework for the future of fatigue crack growth analyses [2]. Implementation of LEFM parameters necessitates limited, localized plasticity within the component. In the event of non-negligible plastic deformation (e.g., extensive blunting of the crack tip or notch), elastic-plastic fracture mechanics (EPFM) parameters must be employed. Computing the path-independent *J*-integral provides a stress field modifying parameter under general plasticity [3]. Shortly after fatigue crack growth analyses implemented fracture mechanics, additional time-dependent analyses were scrutinized.

When cracks propagate under a constant load, time-dependent fracture mechanics parameters are necessary [4]. If the *J*-integral is converted into a rate integral, fracture mechanics approaches can be used to study the rate of cracking in material subjected to constant loads at various temperatures for extended time periods. Crack growth as a result of creep can be readily analyzed utilizing the C^* approach [5]. Advancements during the 1980s extended the C^* approach to include small-scale creep, as well as non-steady-state creep crack growth (CCG), with the C_t parameter [6]. With the more generalized parameters, a variety of CCG conditions have been investigated and characterized independently.

Ideally, simulations and crack life estimations could be made with a single crack growth model encompassing all crack-tip-driving mechanisms. Thus, extending beyond exclusively time-independent or time-dependent crack growth processes and analyses, novel creep-fatigue crack models have been developed to incorporate multiple mechanisms. Recently, approaches for analyzing the effects of creep and fatigue

crack growth simultaneously have been gaining exposure and popularity, with many incorporating fracture-mechanics-based parameters [7,8]. In general, these unified creep-fatigue crack growth models use superposition principles to add the effects that both fatigue and creep have on crack growth. Although they are useful in life estimation, these models typically apply only to long crack growth, disregarding the initiation and short crack growth.

From a fatigue life standpoint, the initiation of a crack in a component is the major factor determining the total life of the component [9,10]. Traditionally, analyses divide the initiation and propagation processes into separate phases and implement different approaches to quantify the total life spent in each [11]. Although fracture mechanics approaches have dominated the fatigue crack propagation stages, a variety of approaches have been proposed to study the initiation of fatigue cracks from notches, including plastic strain and critical plane approaches [12,13]. More commonly, the stress and strain response is approximated by local strain or fracture mechanics approaches [9].

With the success of fracture mechanics parameters in modeling fatigue crack growth rates, the extension to crack initiation has been investigated [14,15]. Implementing fracture mechanics approximations to estimate the true stress concentration, research attempts have been aimed at identifying fatigue crack initiation lives, with limited amounts of success and drawbacks [16]. Improvements to analytical formulations for the stress concentration estimation from fracture mechanics approaches for C(T) specimens following ASTM guidelines have been developed, with maximum errors of approximately 15 % for the most blunted notches [15]. As the notch tip sharpens, the approximation becomes accurate to within 1 %. On this basis, crack initiation processes follow for bluntly notched specimens.

One of the earliest extensions of the fracture mechanics approach to blunted notches arose from observations of stress corrosion cracking (SCC) in aluminum [17]. In studies of dissolution mechanisms related to SCC, it was observed that the crack was more accurately described as a blunted notch, not the typical crack ending with a zero radius of curvature. If the origin is carefully selected to be a distance of $\rho/2$ away from the notch tip, where ρ is the radius of curvature of the notch, the elastic stress field components can be presented in typical fracture mechanics approaches. Utilizing this approach, researchers extended the blunt notch approximation to a C(T) specimen with a keyhole notch by implementing ASTM E399 [18] stress intensity factor calculations to describe crack initiation [14]. Results, in the form of maximum elastic Hookean stress versus crack initiation and fracture life, agreed with Neuber's postulation that the elastic stress at the notch tip controls the fatigue life.

Extending a blocked slip-band model to deep notches in components like that of the C(T) specimen used in Ref 14, researchers developed a notch stress intensity relation to predict initiation [16]. When the strength of smooth specimens is incorporated, the notch factor for fatigue specimens with deep notches can be approximated. The relationship between the relative apparent stress intensity range and the square root of the relative notch-tip radius was observed to correlate well with applied stress intensity ranges and various notch-tip radii. The implication of this relation is that fatigue lives can be readily predicted using fracture mechanics approximations for notched components, resulting in stress-life predictions similar

to those of smooth specimens. Ultimately, this approach was shown to readily capture crack initiation in low-cycle and high-cycle fatigue.

To date, coupled fracture-mechanics-based crack initiation and propagation models emanating from blunt notches have yet to be developed. Coupled initiation and propagation models capable of replicating experimental data and extrapolating to components subjected to fatigue, and potentially creep-fatigue, conditions are imperative to structural life analysis; therefore, it was the goal of this research to develop an advanced deterministic tool to be applied in the design and life analysis of components operating in extreme environmental conditions. A main emphasis is to couple the initiation and propagation of cracks, capturing the events in a single specimen and estimating life based on EPFM approaches. Although the investigation focuses on a specific alloy, 304 stainless steel, the proposed coupled analytical models are intended for a variety of metals utilized in components exposed to elevated temperatures and cyclic loading.

Experimental Approach

The experimental approach taken within the scope of this research was developed to identify key parameters vital to the development of a novel fracture-mechanics-based initiation and propagation life-prediction model. Experimental test matrices were developed based on tensile and fracture mechanics approaches (**Tables 1** and **2**). Specimens were obtained from a single source, namely, a 1.00-in.-thick (25.4 mm) plate of SS 304, as shown in **Fig. 1**.

Tensile testing was required to determine properties of the raw material from which fracture specimens were obtained. The properties determined from the tensile tests were then utilized during the fracture mechanics testing. Parameters used in the fracture test matrix were developed to replicate components that are cycled with short hold periods between loading and unloading within industrial gas turbines. During fracture testing, several monitoring techniques were implemented capable of calculating several fracture mechanics parameters, including K, J, C^*, and others. Based on the results from the tensile and fracture mechanics testing, the dependence on load and material properties essential to the initiation and propagation model was observed and, when warranted, utilized.

Major contributing factors affecting crack initiation and growth, based on the literature and firsthand experience, are presented in **Table 3**. To single out the contribution that the temperature, load, stress ratio, and rise-time-to-hold-time relation have on both initiation and growth, the matrix includes various values so that the effect each has on the material response can be analyzed. Loads were chosen that would result in similar elastic-plastic stress-strain responses at the notch tip, based

TABLE 1

Experimental test matrix of tensile specimens.

Specimen	Temperature T, °F (°C)	Strain Rate, s^{-1}	Specimen Orientation
Ten1	68 (20)	0.001	T
Ten2	600 (315)	0.001	T
Ten3	800 (427)	0.001	T

TABLE 2

Experimental test matrix of blunt notch fracture specimens.

Specimen	Temperature, T, °F (°C)	Maximum Load P, lbf (kN)	Load Ratio R	Rise Time t_r, s	Hold Time t_h, s	Specimen Orientation
BN1	600 (315)	825 (3.67)	0.1	2	2	T-L
BN2	800 (427)	800 (3.56)	0.1	2	2	T-L
BN3	800 (427)	800 (3.56)	0.1	2	20	T-L
BN4	800 (427)	800 (3.56)	0.1	10	100	T-L
BN5	800 (427)	800 (3.56)	0.1	2	10	T-L
BN6	800 (427)	800 (3.56)	0.1	10	50	T-L
BN7	800 (427)	800 (3.56)	0.05	2	20	T-L
BN8	800 (427)	800 (3.56)	0.05	10	100	T-L
BN9	800 (427)	800 (3.56)	0.05	2	10	T-L
BN10	800 (427)	800 (3.56)	0.05	10	50	T-L
BN11	600 (315)	825 (3.67)	0.1	2	20	T-L
BN13	600 (315)	825 (3.67)	0.1	2	10	T-L
BN14	600 (315)	825 (3.67)	0.1	10	50	T-L
BN15	600 (315)	825 (3.67)	0.05	2	20	T-L
BN17	600 (315)	825 (3.67)	0.05	2	10	T-L
BN18	600 (315)	825 (3.67)	0.05	10	50	T-L
BN19	800 (427)	800 (3.56)	0.05	2	2	T-L
BN20	600 (315)	825 (3.67)	0.05	2	2	T-L

FIG. 1

Tensile and fracture specimen orientation in the sheet of raw material.

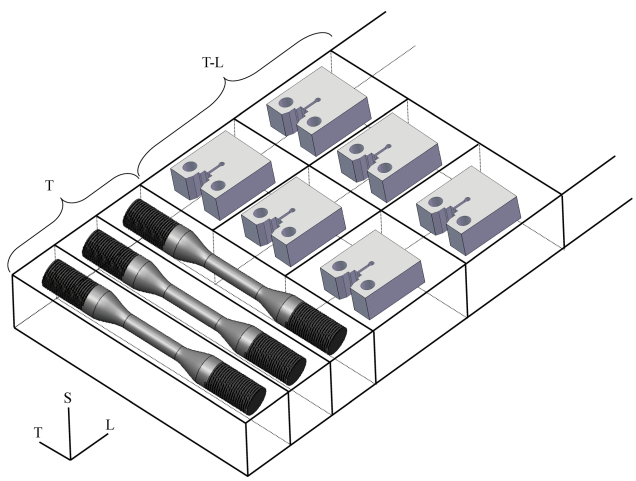

TABLE 3

Optimized crack initiation model constants.

D	p	q
128 894	0.72	4.05

FIG. 2
Load waveform used during crack initiation and propagation experiments.

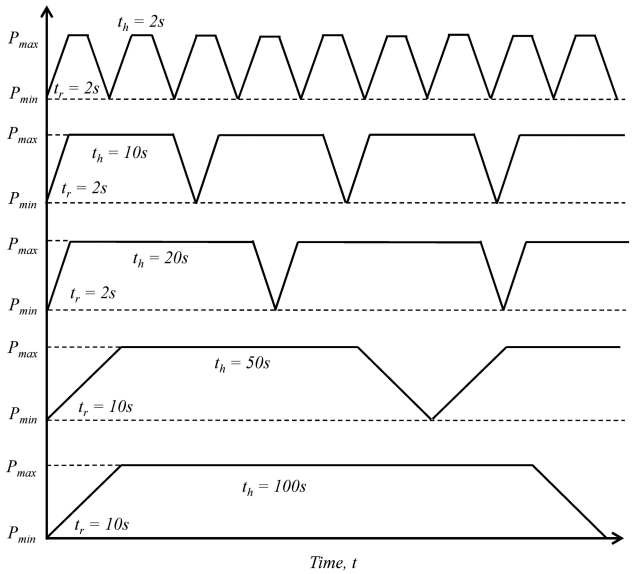

on the results from the tensile tests. The hold times include short and long periods, allowing the evolution of crack growth during hold times to be observed, as shown in **Fig. 2**. Mean stress effects, most commonly accounted for by various *R* values, were to be observed through two slightly different stress ratios. The interaction of hold-time and fatigue effects during load times was accounted for through the load rise conditions. Ultimately, several key parameters in fatigue crack initiation and growth were capable of being experimentally observed through the implementation of **Table 2**.

FIG. 3 Blunt notched fatigue specimen utilized in this investigation.

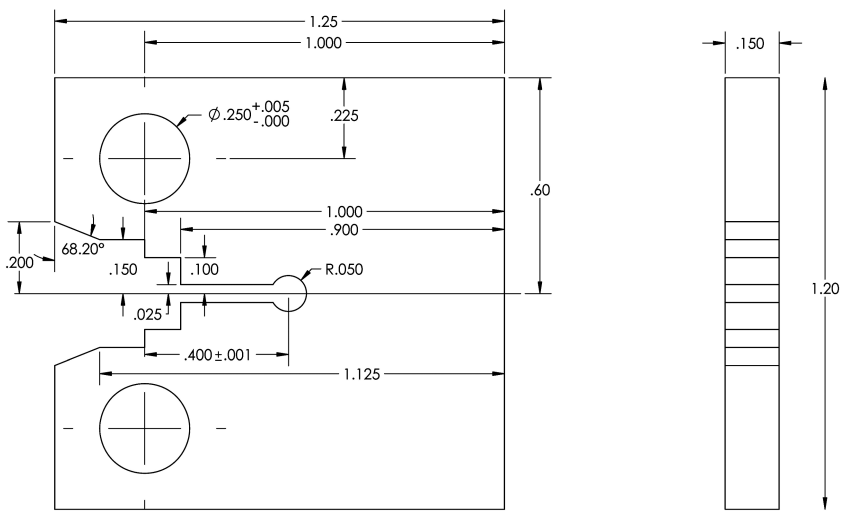

Following ASTM E399 and ASTM E647 [19] as guidelines, a blunt-notch creep-fatigue specimen was designed and implemented, as shown with relevant dimensions in **Fig. 3**. A modification to the notch tip was implemented to simulate a component with a stress concentration similar to that found in service components. Typically, a sharp starter V-notch is machined at the tip to force crack initiation to occur at one location during precracking routines [20]. As this investigation was focused on crack initiation in addition to crack propagation, a blunt notch was used in favor of the V-notch. This allowed the observation and understanding of the manner in which notch and crack tip parameters (e.g., K_t, χ, K, and J) can be applied to the initiation processes of cracks. Additionally, the thickness of the specimen was such that it did not conform to ASTM standards, necessitating the use of an EPFM approach.

Experiments were conducted on an electromechanical load frame controlled via TestWorks v4.12 Creator. Utilizing this universal load frame required the development of both load frame fixtures and test control routines. The necessary load frame fixtures included attachment clevises, extension arms, and a resistance band heater, as defined in ASTM standards [20]. Control routines were developed within the software that monitored and controlled load, displacement, and crack mouth opening displacement (CMOD), as well as the internal DAQ system. Temperature was monitored and controlled via K-type thermocouples welded to the specimen. In situ specimen monitoring of both CMOD and Direct Current Potential Drop (DCPD) crack length measurements required the incorporation of a high-temperature CMOD gauge and the development of a DCPD measurement system. Complete experimental details, with relevant capabilities and limitations, are outlined in Ref 21.

Upon rupture, specimens were observed at various magnifications via conventional microscopy. Macroscopic images of fracture surfaces were obtained from a digital microscope, and sectioned surfaces were etched and viewed under a metallurgical microscope. Greater magnification was achieved with a scanning electron microscope providing typical magnification between 1000 and 1500×, which provided sufficient resolution to identify the key areas of interest, particularly the striation spacing. Coupled with the quantitative data obtained from the mechanical tests, the qualitative data were used to characterize the fracture results and develop the coupled crack initiation and propagation model.

Experimental Results

Elastic and tensile properties for the selected orientation and batch of material were determined from standard tensile tests, as per ASTM E8 and ASTM E21 [22,23]. Tensile tests were conducted at 68°F (20°C), 600°F (315°C), and 800°F (427°C) at a rate acceptable within published standards. Mechanical loading was imposed after an approximately 15-min saturation period in which the specimen was allowed to achieve a stable temperature reading, as reported by thermocouple readings. Results are provided for strains up to 4 % with the associated Ramberg–Osgood material constants (**Fig. 4**).

During all crack initiation and propagation experiments, a significant amount of plasticity was observed, in particular during the first load, as shown in **Fig. 5**. Upon initial loading of the specimen, plastic strains accumulated at the notch tip, resulting in permanent set in the material at the notch. Upon subsequent loading, this effect

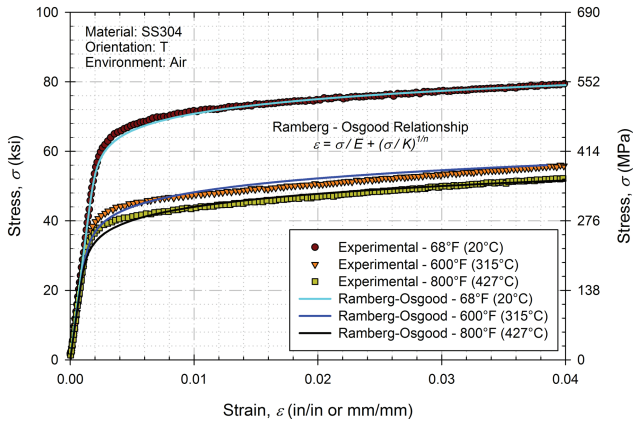

FIG. 4
Expanded view of the stress-strain curves in the low-strain regime with fitted Ramberg–Osgood approximation.

was greatly diminished, with the softening of the material in the notch vicinity completed within the first 50 cycles of the test, as shown in **Fig. 6**. This behavior is representative of structures that may have sharp notches or concentrations in which the material relaxes and the response upon further cycling is linear, such as a component exposed to a thermal load under fixed boundary conditions. Furthermore, **Figs. 5** and **6** were used in calculating both J_1, defined here as the approximated J-integral for the first cycle based on initial notch length, and ΔJ, the cyclic J-integral, based on the experimental method outlined in Ref 24.

The overall amount of plasticity observed in the experiments was extensive, as demonstrated by the evolution of the load versus load-line deflection response for the entirety of a test provided in **Fig. 7**. Excluding the first and last few cycles of a test, however, the amount of cyclic plasticity was small. As a result of the small cyclic plasticity, approximations to ΔK could have been made, as in Ref 24; however, due to the existence of hold periods and the overall plasticity observed, such an approximation was not made in this investigation. The choice was further aided by the

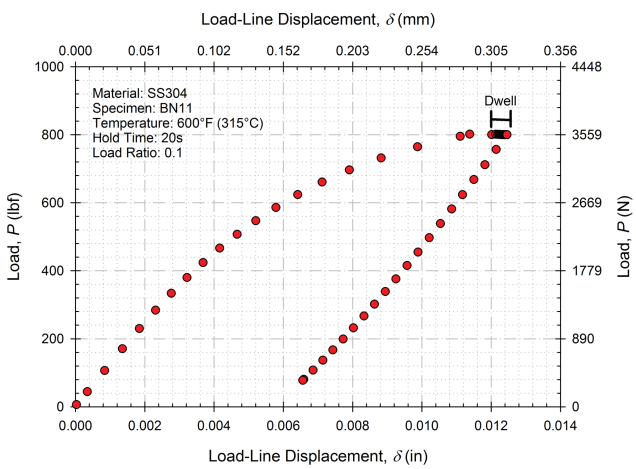

FIG. 5
Nonlinear behavior in the curve of load versus load-line displacement for the first cycle of a creep-fatigue specimen, BN11.

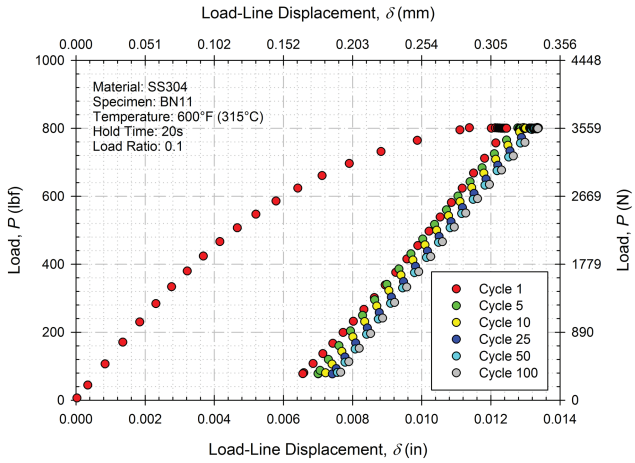

FIG. 6
Example of the load versus load-line displacement for the first 100 cycles of specimen BN11 from **Fig. 5**

physical appearance of the tested specimens, in which extensive amounts of plasticity were observed, as shown in **Fig. 8**.

Crack initiation was based on criteria involving the use of a bisection method that fits straight lines to the slope of the steady-state and unstable portions of a measurement [21]. The two generated lines then intersect at a particular point, creating an angle between the two lines. This angle is then bisected with a third line that bisects the previous angle in half and intersects the experimental data curve. The corresponding cycle at which the third generated line intersects the data is then the cycle at which crack initiation is assumed. An example of this method is provided in **Fig. 9**. The measurement signal utilized was the derivative of the CMOD gauge displacement with respect to the change in cycles. Results based on this criterion for the bisection of the steady-state and unstable slopes in the derivative of the CMOD displacement with respect to the change in cycle provided consistent results [21]. If this method is to be applied, a calibration specimen must be tested, enabling a

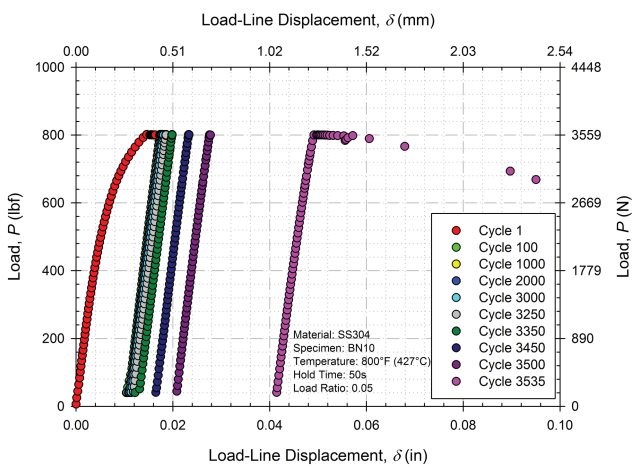

FIG. 7
Example of the load versus load-line displacement for the entirety of a test during crack initiation and propagation experiments, with data from BN10 with 50 s of tensile hold.

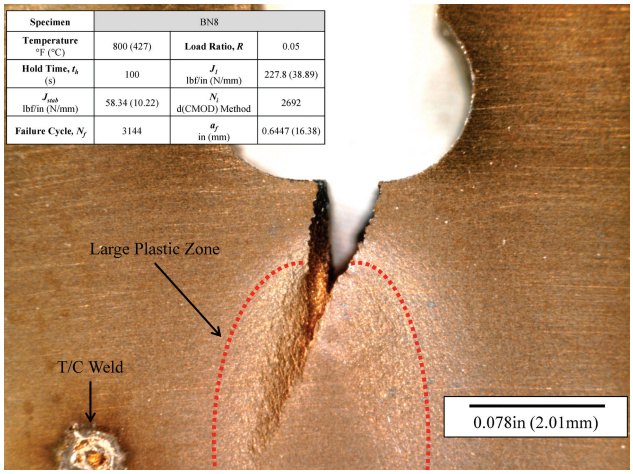

FIG. 8
Example of the large-scale plasticity observed during the duration of a single crack initiation and propagation experiment.

correlation to the crack length at the corresponding crack initiation cycle (e.g., using overload cycles periodically).

As shown in **Fig. 5**, a significant amount of plasticity was observed in the first cycle, resulting in the identification of the aforementioned J_1 value. Saturation of the approximated value of J for the first cycle was observed based on the tensile hold period, with the exception of one outlier, as shown in **Fig. 10**. As the hold time in experiments was increased, the minimum value of J_1 was observed to trend higher toward an upper limit that was dependent on the maximum load of the tests and the extent of relaxation of the material during the initial cycle hold period. The identification of an upper limit suggests that accelerated experimental routines, in which abbreviated hold periods are used to replicate longer exposure times in service, can be developed. By identifying an upper limit, investigators are able to conduct experiments in which excessively long hold periods can be avoided, with the caveat that environmental damage mechanisms (e.g., stress-assisted grain boundary oxidation in nickel alloys) could require more targeted testing. This results in the ability to

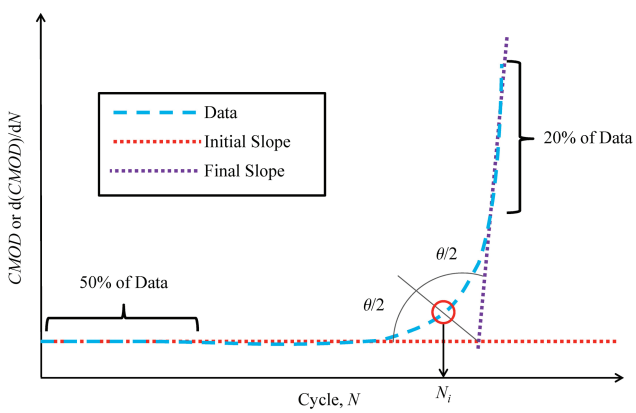

FIG. 9
Example of crack initiation determination based on the bisection method utilizing the slopes of the steady-state and unstable portions of the derivative of the CMOD gauge displacement with respect to the change in cycles.

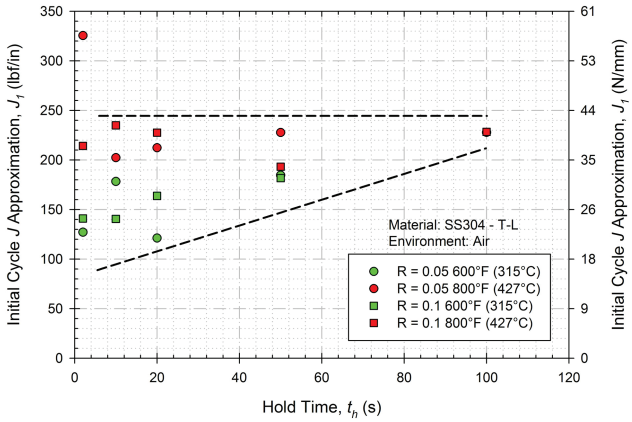

FIG. 10
Saturation of the calculated J for the first cycle based on the tensile hold period during experiments.

conduct shorter tests, driving the financial burden of testing down, potentially leading to additional testing being conducted with additional parameters of interest.

The saturation of a consistent J_1 for the two temperatures is apparent in **Fig. 10**. The tests conducted at a higher temperature showed a higher level of saturation, as well as a higher initial J_1 approximation. Temperature dependence can be argued; however, the increased J_1 approximation for identical conditions aside from temperature could also be used to account for the temperature dependence without explicitly including a temperature-based component. The saturation is expected to be dependent on the level of J imparted to the specimen, and thus a few exploratory tests would be necessary to determine the saturation limit; however, once it is defined, subsequent experiments can utilize the existence of the upper limit. In the case of the outlier, BN19, a software malfunction resulted in a higher-than-expected first cycle load, contributing to the errant result.

Crack initiation was observed to be primarily dependent upon the load ratio R and the approximated value of J for the first cycle J_1, as shown in **Figs. 11** and **12**. As

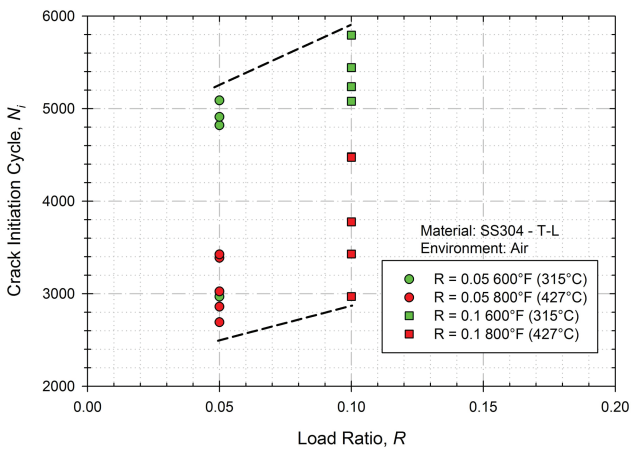

FIG. 11
Load ratio effect on the crack initiation, in which the lower load ratio produced a shorter life to crack initiation.

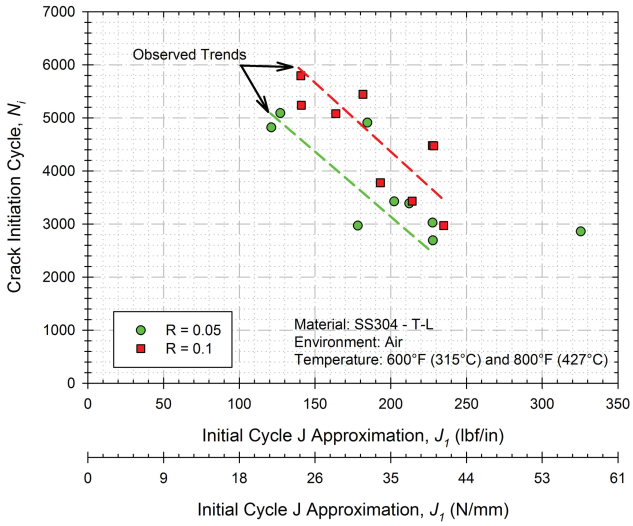

FIG. 12
Crack initiation based on the calculated J for the first cycle at the two load ratios implemented in experimental routines.

the load ratio increased from $R = 0.05$ to $R = 0.1$, the number of cycles required to generate a crack increased, as in **Fig. 11**. Temperature appears to have an effect on the number of cycles to crack initiation; however, as with the saturation of J_1 in **Fig. 10**, the value obtained for J increased at the higher temperature, therefore taking into account the temperature dependence, as shown in **Fig. 12**. A larger load ratio implies a smaller stress range at the notch tip; thus a larger number of cycles is expected to generate a crack. Essentially, this relates back to the traditional S–N or ε–N diagrams for fatigue life analyses in which smaller ranges result in longer lives of components. Ignoring the mean stress effect, as little difference in the initial cyclic J value is observed, this is the effect that is observed within the initiation lives with respect to the load ratio.

When comparing the approximated value of J for the first cycle to the number of cycles to crack initiation, an increase in the load ratio results in a larger J approximation for the same number of cycles at the lower load ratio, as in **Fig. 12**. A trend is also reported, shown as a dashed line, representing the observed behavior with regard to the number of cycles to crack initiation. The approximation of J_1 depends upon the specimen, the measured displacement, the load, and the hold time. The experimental values of J_1 are greater than the numerical predictions in Ref 21; however, the numerical simulations did not incorporate a hold time. By incorporating a more complex material model into numerical simulations, the hold time effects can be accounted for and values of J_1 are expected to correlate very well with experimental data.

Crack growth curves, beginning from the cycle at which crack initiation was identified, were generated based on routines for standard fatigue crack growth analyses [19]. The main factors affecting the rate at which cracks propagated included the temperature, load (or stress) ratio, and characteristics of the load waveform. Crack growth curves are provided based on temperature, load ratio, hold time, and rise time to hold time, shown in **Figs. 13–16**, respectively.

FIG. 13 Crack growth rate curves at 600°F (315°C) and 800°F (427°C).

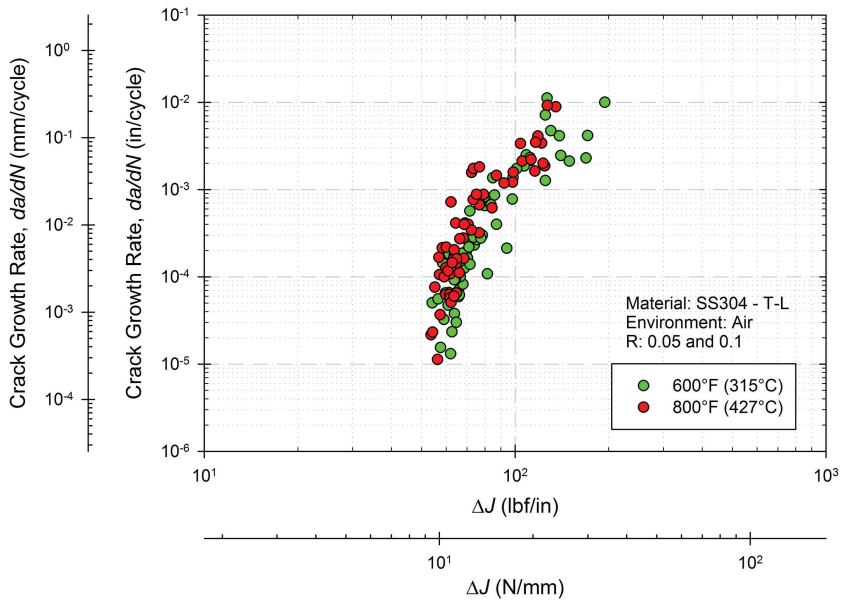

Cumulative crack growth curves based on growth per cycle at 600°F (315°C) and 800°F (427°C) are provided, as shown in **Fig. 13**. A total of 18 specimens are represented, with 8 experiments at 600°F (315°C) and 10 experiments at 800°F (427°C). Crack growth curves are presented without regard to the load ratio or the

FIG. 14 Crack growth rate curves for load ratios of R = 0.05 and R = 0.1 at both test temperatures.

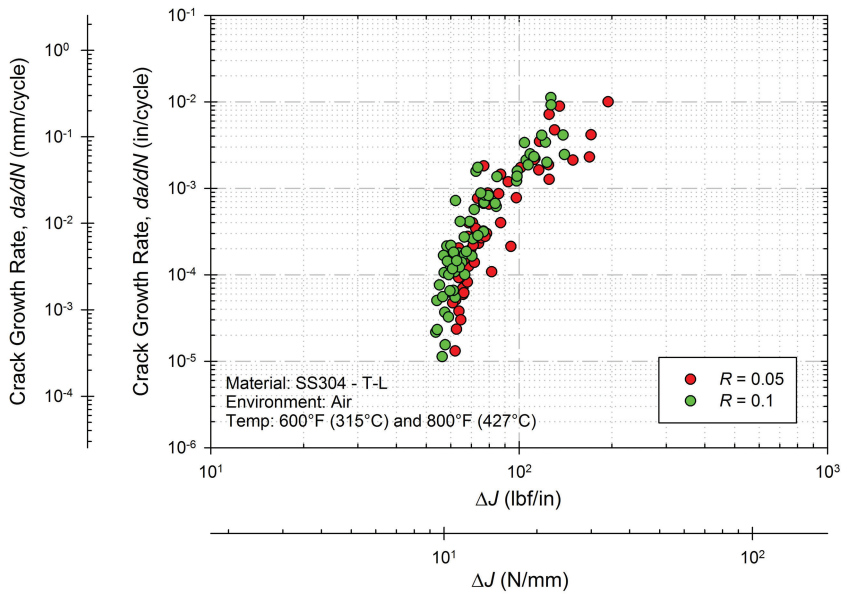

FIG. 15 Crack growth rate curves based on the duration of a positive tensile hold period for both test temperatures.

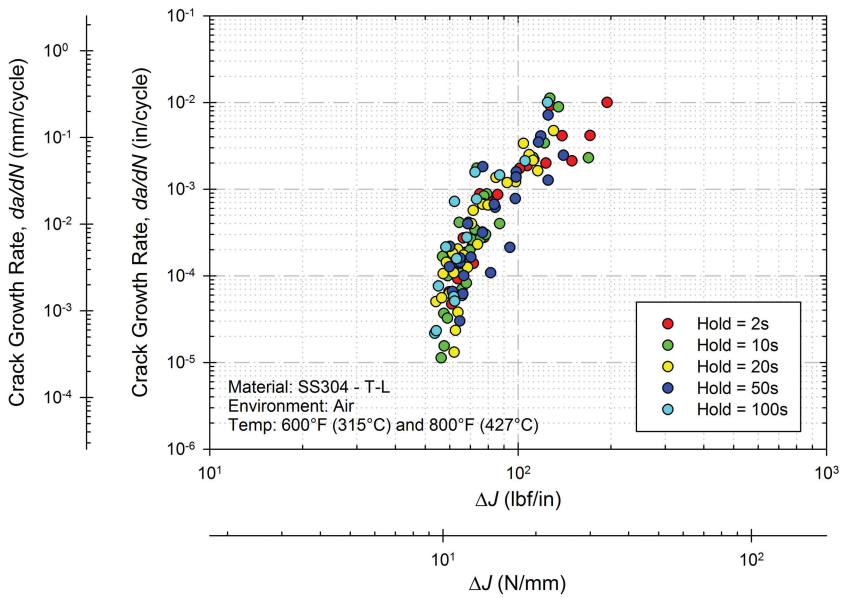

tensile hold period. As in standard fatigue crack growth experiments, the temperature was expected to result in an increase in the crack growth rate; however, only a small distinction between the two temperatures was apparent when utilizing EPFM parameters, with a slightly increased crack growth rate at higher temperatures. This

FIG. 16 Crack growth rate curves based on the ratio of load rise time to hold time.

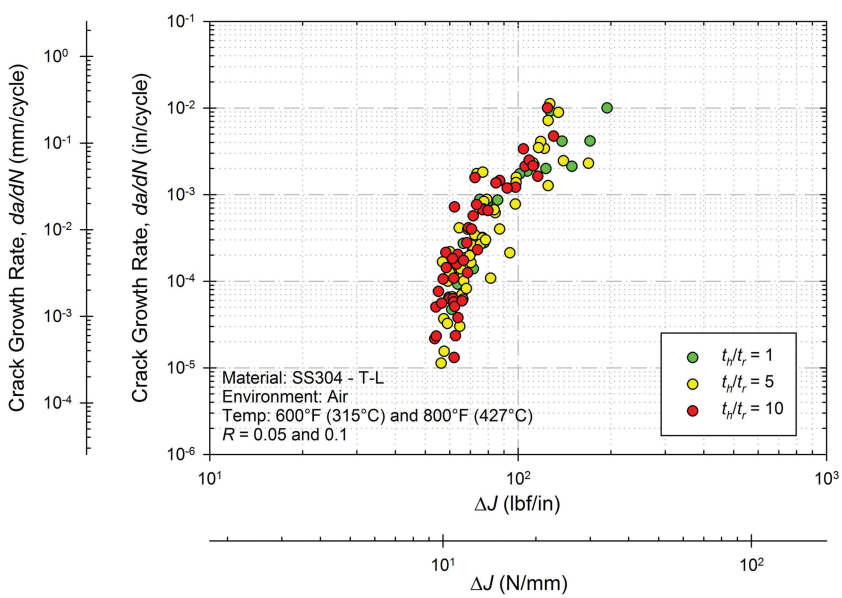

is attributed to the similarity in behavior at the two test temperatures and the change in maximum load at each test temperature, with the tests at lower temperatures having a higher maximum load. Maximum loads were chosen for each temperature in a manner that would result in similar notch tip conditions for all specimens, irrespective of temperature. Because we provided a consistent notch condition regardless of temperature, it was expected that the influence of other parameters modifying crack growth rate would be exaggerated.

Cumulative crack growth rate curves based on growth per cycle at load ratios of 0.05 and 0.1 are provided in **Fig. 14**. A total of 18 specimens are represented, with nine experiments cycled at an R of 0.05 and nine experiments cycled at an R of 0.1. Crack growth curves are presented without regard to the test temperature or the tensile hold period. Irrespective of the temperature, hold time, or rise time, as the load ratio was increased, the trend was that the crack growth rate curve shifted left slightly, resulting in a lower ΔJ required to grow cracks at the same rate. This effect was expected, as the rate of crack propagation has been experimentally proven to be dependent on the load ratio implemented during testing relating back to the amount of crack closure, and this is expected to become more apparent at higher load ratios [25–27]. The small increase in load ratio, which related to approximately a 40-lbf (178-N) difference in minimum load, was enough to reveal the effect the load ratio has on crack propagation rates subjected to the load waveforms implemented in this study. The difference in crack growth rates based on the load ratio necessitates that the proposed model have a dependence on the load ratio used to accelerate crack growth rates at higher load ratios.

Cumulative crack growth curves based on hold time, obtained for both temperatures, are provided in **Fig. 15**. A total of 18 specimens are represented, with four experiments incorporating a tensile hold period of 2 s, four with a tensile hold period of 10 s, four with a tensile hold period of 20 s, four with a tensile hold period of 50 s, and two with a tensile hold period of 100 s. Crack growth curves are presented without regard to the test temperature or the load ratio.

Inspection of the crack growth curves based on the positive tensile hold yields little to no clear differentiation between the datasets. Initially, it was thought that the temperatures and the loads would result in accelerated crack growth rates for longer hold periods in terms of growth per cycle, which would be clearly discernible. The effect of hold time on the creep-fatigue crack growth rates was expected to shift the curves to the left, similar to the effect raising the load ratio R has on crack growth rates. A proposed explanation is that the method of calculating ΔJ, based on integrating the load versus load-line displacement, readily captures the effects of hold time for a given initial crack length, as any additional displacement due to longer hold times is captured by the bounds of the integration. The total area under the curve is calculated, taking additional displacements due to hold period crack extension into account.

In addition to the hold-time-based crack growth rate, rates were inspected based on the ratio between the load rise and hold time, as shown in **Fig. 16**. Again, a clear distinction between experiments with hold–rise time ratios of 1, 5, and 10 was not readily achieved. The lack of correlation is proposed to be similar to the assessment that the implemented J calculation inherently includes the effects of hold time on the crack growth rates. Any notable effects based on the rise–hold time ratios

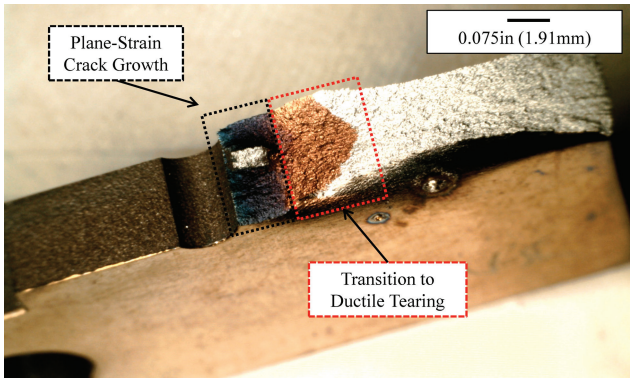

FIG. 17
Transition from plane-strain crack growth to extensive plasticity and ductile tearing.

are accounted for in the calculation of J and remain dependent on the applied load ratio.

All experiments were stopped prior to complete specimen rupture, as hardware limits were reached as a result of the extensive plasticity and transition to ductile tearing near the end of life. Subsequent separation of the specimens revealed the fracture surfaces, and upon viewing under the digital microscope, we were able to measure crack lengths. Because of the elevated temperatures, heat tints were highly visible for samples tested at both temperatures (e.g., **Fig. 17**). Using the heat tint on the surface as a reference, crack lengths were readily measured, using the tip of the heat tint as the maximum length. Additionally, the heat tints served to validate the test temperatures at which tests were conducted, with color bands similar to those found in the literature for the test temperatures used in this investigation

Fracture surfaces within the heat-tinted area (i.e., the region of crack initiation and propagation) were predominantly flat, with minimal deviation from the plane normal to load application. The absence of shear lips within this region provided evidence that plane strain conditions prevailed at the notch tip and for the majority of crack propagation. A transition was readily observed in that extensive shear lips dominated toward the end of life, as shown in **Fig. 17**. Although the specimen thickness violated the standard thicknesses outlined in ASTM standards for fatigue and CCG experiments, states of plane-strain crack growth were present. In the event that EPFM crack growth data are unavailable, using the approximation of LEFM parameters from EPFM parameters is warranted for the current load and environment combination.

Scanning electron microscopy was used to inspect the surface of several ruptured specimens, with primary goals of distinguishing the modes of fracture and observing indications of fatigue damage. Major differences in the general appearance of fracture surfaces of specimens tested at the two elevated temperatures were not readily observed [21]. The fracture surfaces exhibited flat surfaces near the notch where cracks were grown as a result of the imposed loading schemes. Cracks were observed to initiate at the root of the notch in the desired location. In some cases, multiple cracks initiated at various distances from the dominant crack plane along

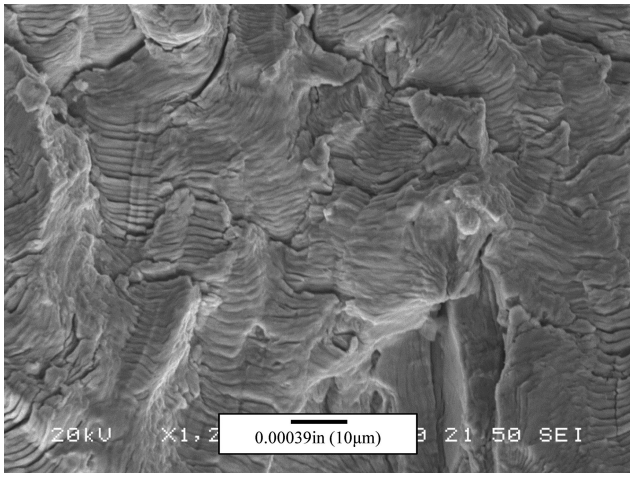

FIG. 18
Fatigue striations on the surface of large flakes observed on the fracture surface of BN6.

the thickness of the notch root; however, cracks were observed to coalesce to a single crack within the plane-strain crack plane region (**Fig. 17**).

Striation spacing was readily measured on the surface of specimens in both early and mid-stages of crack growth, as shown in **Fig. 18** [21]. In the early stages of crack growth, striation spacing was typically 0.00001 in. (0.254 μm), and mid-life striation spacing was on the order of 0.0001 in. (2.56 μm) to 0.0006 in. (15.2 μm). In both cases, the spacing correlated with the crack growth rates reported in **Figs. 13–16**. Late-stage crack growth was observed to transition from fatigue-dominant failure to ductile tearing, as noted previously, resulting in crack growth rates that were larger than anticipated. The observation of the spacing and transition to ductile tearing toward the end of the crack length confirmed that larger-than-normal crack growth rates were present as a result of the extensive plasticity occurring.

A transition was observed from the fatigue-dominated regime to a regime of ductile tearing (e.g., the surface of BN11) as shown in **Fig. 19**. Upon further

FIG. 19 Transition region (left) from crack growth to ductile tearing on BN11 tested at 600°F (315°C) with a tensile hold of 20 s, with a magnified view provided (right).

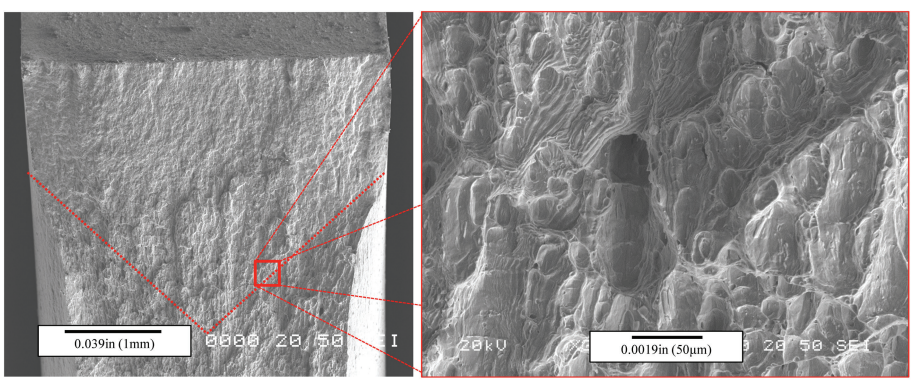

magnification of this region, the presence of striations and the introduction of ductile dimples were noted, confirming that there was a transition of the failure mechanism toward the end of the life of the specimen. This is expected, as the crack length begins to extend to lengths that will result in instability and ductile tearing. These regions, which correlated with the digital microscopy, also served to confirm the crack lengths measured optically.

Model Correlations

CRACK INITIATION MODEL

In the development of the crack initiation model, several influencing factors were considered and evaluated. Relationships among the test temperature, load ratio, rise time, hold time, and notch tip stress-strain modifying parameters were sought. Of all the influential factors observed, the most prominent factors observed to correlate with the number of cycles to crack initiation were the load ratio and the approximation of J for the initial loading cycle. Temperature was found to be inconsequential, as the softening at higher temperatures was accounted for in the approximate calculation of J and additional softening was accounted for through the additional load-line displacement.

To reproduce the trends observed in **Fig. 12**, a balance was desired that would allow us to adequately capture the experimental behavior while maintaining a form that was easily understood and implemented. Power-law-based analytical modes (e.g., Paris law) are commonly used in phenomenological models because they have the ability to replicate experimental behavior with limited complexity. Therefore, we implemented a power law, and the proposed empirical crack initiation model is

$$N_i = \frac{D}{(J_1)^p (1-R)^q} \tag{1}$$

where:

J_1 = approximated J-integral calculated from the initial load cycle,
N_i = number of cycles to crack initiation,
R = load ratio, and
D, p, and q = fitting constants.

Equation 1 requires material constant determination, outlined in detail in Ref 21, in addition to the calculation of J_1 and N_i from experimental data.

The main assumption of the model proposed in Eq 1 is that the presence of a notch constitutes a crack-like feature. In the experimental portion of this investigation, crack initiation was observed to occur at the root of the notch, providing the necessary condition for Eq 1 to be applicable. No constraints were applied with regard to the maximum crack length or the load type, as the crack length is to be defined during the experimental portion and the load is inherently taken into account by the calculation of the proposed J_1 approximation. It is intended that this value of J_1 be calculated via finite element analysis, as analytical solutions may be challenging for typical life analyses. Extension of this model to smooth or other experimental geometries will require the use of appropriate specimen geometries capable of demonstrating initiation and small crack propagation.

The main advantage of Eq 1 in crack initiation life estimation analyses is the simplicity of the requisite parameters. Upon the completion of experimental testing and constant determination for a given material, merely calculating the approximated value of J_1 at a crack-like location within an elastic-plastic finite element simulation has the ability to predict the number of cycles to crack initiation. In most cases, the load ratio would be nearly zero depending on the extent of plasticity, as in the case of a "peaker"; however, crack initiation predictions can readily be made at any load ratio for which experimental data have been obtained for set load conditions. Although the length of the crack that defines initiation is open to interpretation, Eq 1 is adaptable to any length as defined by the investigator.

CRACK PROPAGATION MODEL

The proposed crack propagation model, similar to the proposed crack initiation model, follows suit in that power law behavior is noted. The proposed model incorporates multiple terms to account for the three stages of crack growth observed within this investigation.

$$\frac{da}{dN} = \frac{C\left(1 - \frac{\Delta J_{stab}}{\Delta J}\right)^a}{(\Delta J)^b[(1-R)J_c - \Delta J]^c} \tag{2}$$

where:

ΔJ_{stab} = threshold-like asymptote for Stage I crack growth,
ΔJ = cyclic J-integral,
J_c = critical-like asymptote for Stage III crack growth,
R = load ratio, and
C, a, b, and c = fitting constants.

Each term with an exponent is targeted to capture a particular stage of crack growth.

Model development began with the Stage II crack growth (i.e., the linear portion of crack growth on a log-log scale). As pioneered by Paris for LEFM parameters, the crack growth rate per cycle was observed to be a function of the cyclic EPFM J-integral [1].

$$\frac{da}{dN} \propto C(\Delta J)^b \tag{3}$$

To incorporate the increased rates of Stage III crack growth, the load ratio R and the critical-like asymptote J_c for instability were incorporated, similar to what is described in Ref 25.

$$\frac{da}{dN} \propto \frac{1}{[(1-R)J_c - \Delta J]^c} \tag{4}$$

Stage I crack growth rate dependence incorporated the threshold-like asymptote ΔJ_{stab}, similar to what is described in Ref 28.

$$\frac{da}{dN} \propto \left(1 - \frac{\Delta J_{stab}}{\Delta J}\right)^a \tag{5}$$

The final form of the proposed crack growth model, as shown in Eq 2, is a combination of Eqs 3–5 capable of simulating the crack growth rates in materials subjected to elastic-plastic loads.

Two of the parameters in the proposed model, ΔJ_{stab} and J_c, are plastic variations of the threshold stress intensity factor K_{th} and the critical or plane-strain fracture toughness K_c, respectively. In LEFM, K_{th} is an experimentally obtained minimum value at which cracks are not expected to propagate when ΔK is below. The plastic variation presented here, ΔJ_{stab}, is the approximation of the cyclic J-integral to which the uncracked component is subjected over the majority of its life. It is not a threshold below which cracks do not grow; rather, it is a parameter that relates to the stress and strain at the blunted notch that subsequent crack propagation predictions use as the initial ΔJ. When this is inserted into Eq 2, the asymptotic behavior and faster crack growth rates for small cracks can accurately be modeled.

Accelerating the crack growth rates closer to the instability region, J_c is the plastic variant of the critical stress intensity or the plane-strain fracture toughness, K_c or K_{Ic}, respectively. Under LEFM crack growth analyses, this parameter serves as the asymptote for crack growth rates with respect to ΔK and is the measured instability for the material. In the elastoplastic analysis conducted, a plastic variation of this value, J_c, is used in a similar manner. As the value of ΔJ approaches the value of J_c, crack growth rates are observed to increase at an increasing rate. When this value is incorporated in Eq 2, the acceleration of crack growth rates is captured.

Accurate replication of the experimental data utilizing Eqs 1 and 2 requires the determination of material constants. As with all mechanical models, either mechanistic or phenomenologically based, the constants will be dependent upon the material and environment. In the current state, neither Eq 1 nor Eq 2 is temperature dependent, as the approximation of the J-integral approach taken inherently accounted for the temperature dependence. Future testing should be conducted to investigate the effect of temperature on the proposed initiation and propagation models, as a dependence could be uncovered over larger ranges for different materials. Nevertheless, both of the proposed models were fit to the experimental data, with constants listed in **Tables 3** and **4**, resulting in the curves overlaid on experimental data in **Figs. 20** and **21**.

Both crack initiation and propagation models predict and replicate the experimental data to a degree with limited amounts of variability, as shown in **Figs. 22** and **23**. In **Fig. 22**, the correlation for the crack initiation cycle includes error bars that are a factor of ±25 %, whereas **Fig. 23**, regarding crack growth rates, includes error bars that are a factor of ±2. Using the R^2 error metric, the crack initiation model has a value of $R^2 = 0.705$ and the crack propagation model has a value of $R^2 = 0.913$. Model correlation coefficients with the experimental data for both the initiation and propagation models were observed to be 0.840 and 0.891, respectively.

TABLE 4

Optimized crack propagation model constants.

C	a	b	c	J_c
281	2.08	1.07	1.08	240

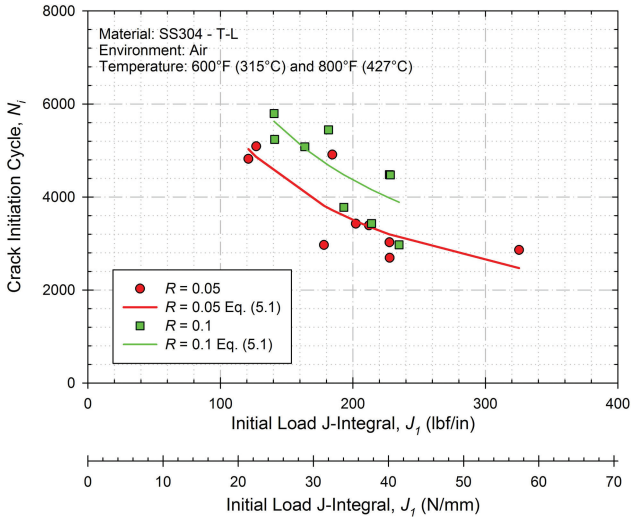

FIG. 20
Experimental and predicted crack initiation results using the proposed fatigue crack initiation model.

As observed in the application of current models, the scatter in data is common even with models that utilize more complex formulations and require more parameters to furnish predictions. This scatter can be related back to the experimental data and the constants used to fit the data. For the optimized set of constants, crack growth rates were observed to be nonconservative toward the end of life, as shown in **Fig. 23**. This is a direct result of the sampling rate limitation of the software, as noted in Ref 21. Ultimately, a balance of simplicity and accuracy is maintained by using both the proposed initiation and propagation models, in which conservative life predictions can be made by applying small debits or credits to the end of life, outlined in Ref 21.

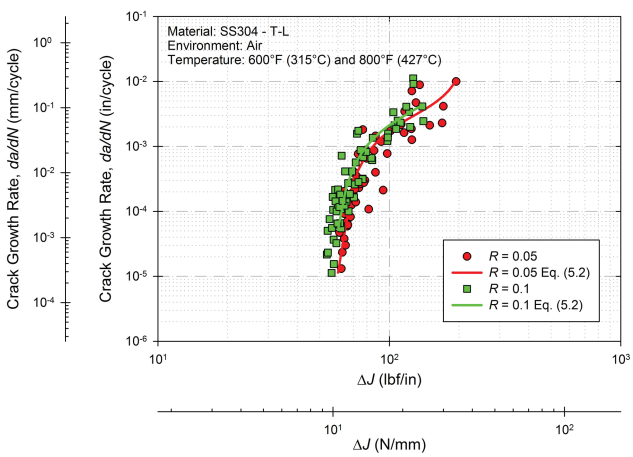

FIG. 21
Experimental and predicted crack propagation results using the proposed fatigue crack propagation model.

FIG. 22
Correlation of crack initiation life using the proposed fatigue crack initiation model on SS304 at 600°F (315°C) and 800°F (427°C).

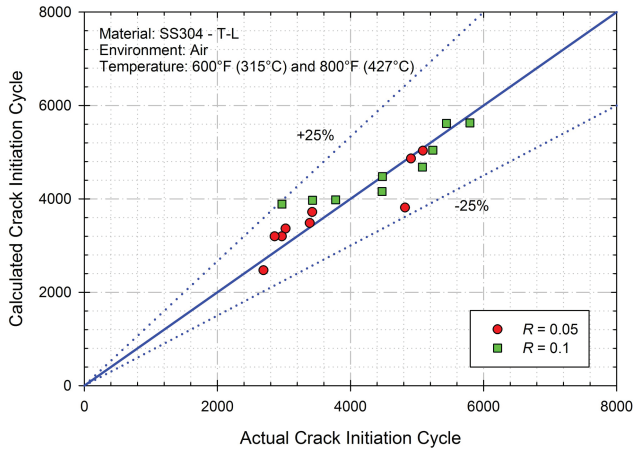

CRACK INITIATION AND PROPAGATION MODEL IMPLEMENTATION

The intended application of the crack initiation model is the structural analysis of components and necessitates the use of an elastic-plastic finite element simulation. A material model must be selected and can be either a standard model within the software package or a custom user-developed model. Suitable constitutive material models include multilinear kinematic hardening and viscoplastic models (e.g., Chaboche or MATMOD models). By implementing an advanced material model with plasticity, one can accurately simulate the behavior after softening or hardening

FIG. 23 Correlation of crack propagation rates using the proposed fatigue crack propagation model on SS304 at 600°F (315°C) and 800°F (427°C).

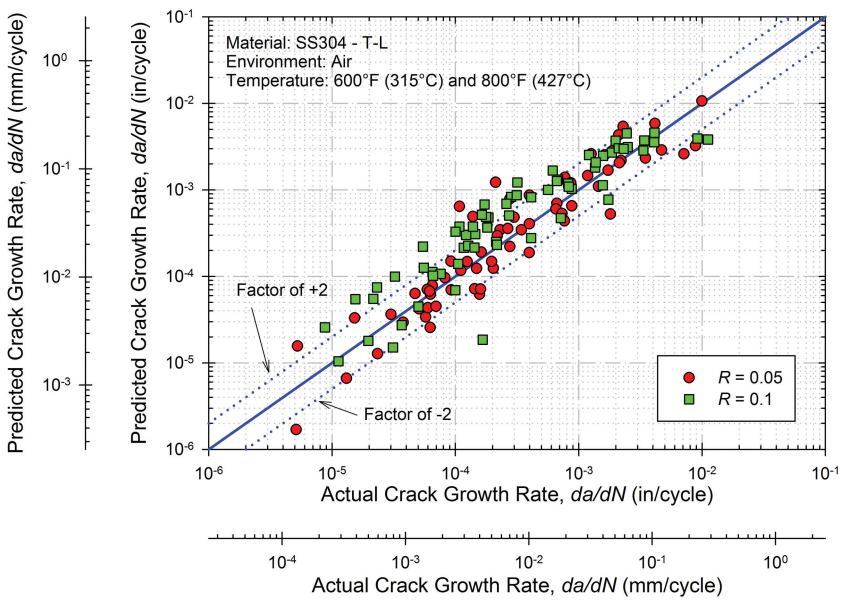

effects, establishing the baseline for the ΔJ_{stab} parameter used in the crack propagation model.

Locations with a significant stress concentration and the potential for yielding upon initial loading, such as the transition from a blade platform to a blade, shall be modeled and meshed with suitable refinements. With refinement around the location of interest, a smaller deviation in the contour integral calculations is expected. Although the *J*-integral is theoretically path-independent, some dependence is observed in elastic-plastic analyses. To minimize the amount of variation, simple simulations should be run with various levels of refinement at the key area. As the values obtained from the *J*-integral converge, a suitable mesh is achieved and full simulations should be conducted.

With the appropriate boundary conditions applied to the model, simulations should be conducted to estimate the response after the first cycle. Once the value of the approximate *J*-integral around the area of interest has been obtained, crack initiation estimations can be made from this value and the load ratio of subsequent cycling. Crack lengths that define crack initiation are to be defined by the user, as they will depend on the monitoring technique, the resolution of the monitoring devices, or the standard length defined by the governing body of the investigator. This value is to be set prior to structural assessment analyses in particular during the experimental investigation and is subsequently used in the material constant determination process. With the model calibrated to the material and a fixed length defining initiation, the number of cycles to crack initiation is readily calculated, as outlined in **Fig. 24**.

FIG. 24 Schematic of suggested implementation routine for the proposed crack initiation model.

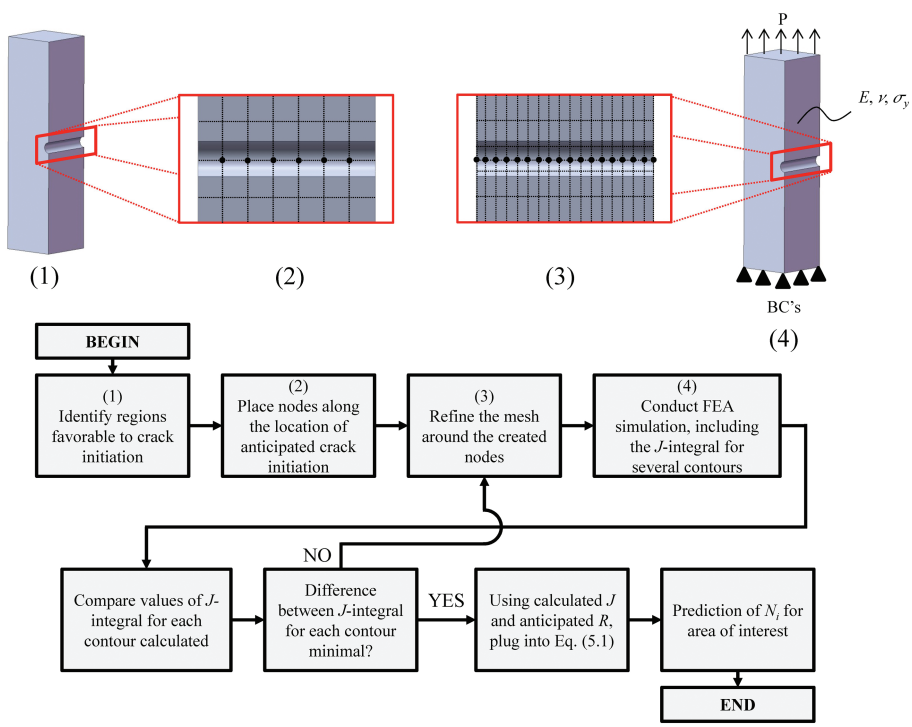

FIG. 25 Schematic of suggested implementation routine for the proposed crack propagation model.

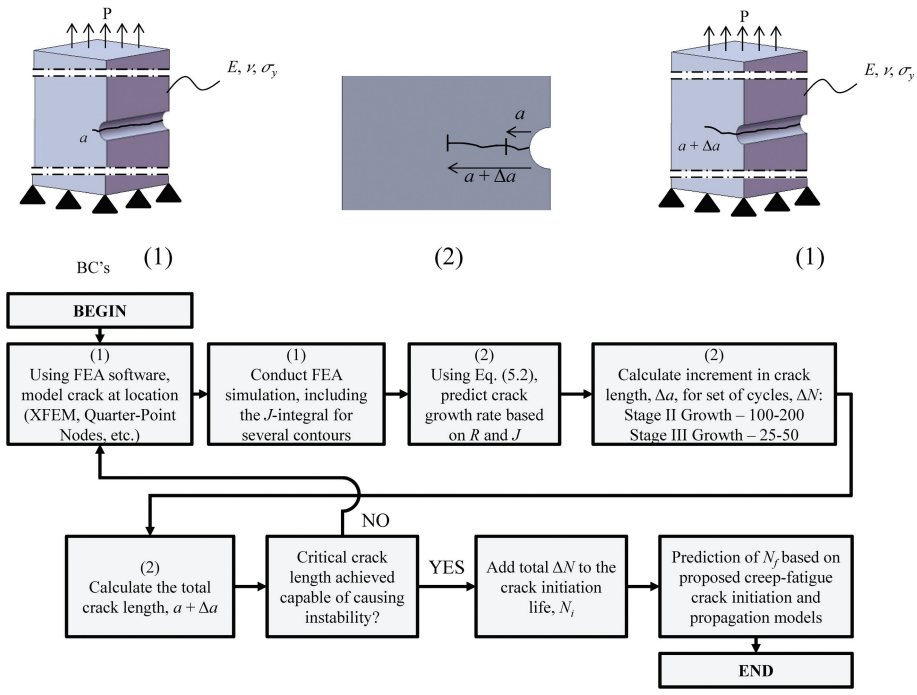

Once the crack initiation life has been reached, the crack propagation portion of the analysis can be completed in a number of fashions, ranging in complexity. Following the initiation of a crack, a quick approximation to determine the number of cycles until failure is to integrate the proposed model in Eq 2 between the current crack length and the critical crack length. This is likened to the effect of using a Paris law for Stage II crack growth to simulate the accumulation of length over all stages of crack growth. This method, although straightforward and expedient, will ultimately lead to an overapproximation in life, as it does not take into account the increase in crack growth rates as the value of ΔJ increases with increasing crack lengths. As a result, an iterative process for determining the remaining life is necessary.

For a more accurate, conservative approach, a multistep process is suggested, as outlined in **Fig. 25**. First, one should calculate the approximate J for the initial crack length. Using the initial length, the approximate ΔJ value, and the load ratio, the crack growth rates are summed over a set of cycles (e.g., 100 to 200 cycles for early stages of crack growth). Next, the initial crack length is extended by the total Δa as a result of the growth over the set of cycles, and a new value of ΔJ is obtained. Again, the corresponding crack growth rate for this value of ΔJ is obtained and crack growth rates are summed. This process is repeated until the critical crack length of the subject material is approached, and the number of cycles in a set in which Δa is approximated should be decreased to accurately account for the transition from Stage II to Stage III crack growth. An iterative crack propagation study will

provide more accurate total life predictions with a lesser probability of being nonconservative.

Summary

The development of a comprehensive crack initiation and propagation model included the use of a modified fracture specimen used in an experimental setup capable of imparting conditions similar to those found on the subject SS304 in service conditions. Incorporating both the initiation and propagation stages, two phenomenologically based models were proposed to be used in tandem to predict the total life of a component subjected to various load waveforms at elevated temperatures. Both the crack initiation and the propagation models are observed to be based upon the EPFM parameter J and the load ratio R, capturing the effects that both fatigue and creep have on the total life of the component. Material constants were observed to be independent of temperature, requiring minimal parameter determination and optimization. Implementation into routine structural analyses is straightforward, enabling the models to be used in standard life prediction routines with limited amounts of additional work.

References

[1] Paris, P. C., Gomez, M. P., and Anderson, W. E., "A Rational Analytic Theory of Fatigue," *Trends Eng.*, Vol. 13, 1961, pp. 9–14.

[2] Paris, P. C., "Fracture Mechanics and Fatigue: A Historical Perspective," *Fatigue Fract. Eng. Mater. Struct.*, Vol. 21(5), 1998, pp. 535–540.

[3] Rice, J. R., "A Path Independent Integral and the Approximate Analysis of Strain Concentration by Notches and Cracks," *J. Appl. Mech.*, Vol. 35, 1968, pp. 379–386.

[4] Landes, J. D. and Begley, J. A., "A Fracture Mechanics Approach to Creep Crack Growth," *Mechanics of Crack Growth, ASTM STP 590*, J. R. Rice and P. C. Paris, Eds., ASTM International, West Conshohocken, PA, 1976, pp. 128–148.

[5] Saxena, A., Williams, R. S., and Shih, T. T., "A Model for Representing and Predicting the Influence of Hold Time on Fatigue Crack Growth Behavior at Elevated Temperature," *Proceedings of Fracture Mechanics: Thirteenth Conference, ASTM STP 743*, R. Roberts, Ed., Philadelphia, PA, June 16–18, 1980, ASTM International, West Conshohocken, PA, 1981, pp. 86–99.

[6] Saxena, A., "Creep Crack Growth under Non-Steady-State Conditions," *Fracture Mechanics: Seventh Volume, ASTM STP 905*, J. H. Underwood, R. Chait, C. W. Smith, D. P. Wilhem, W. A. Andrews, and J. C. Newman, Eds., Albany, NY, Aug 7–9, 1984, ASTM International, West Conshohocken, PA, 1986, pp. 185–201.

[7] Baik, Y. M. and Kim, K. S., "Crack Growth in Stainless Steel 304 Under Creep-Fatigue Loading," *Key Eng. Mater.*, Vol. 353(1), 2007, pp. 485–490.

[8] Zhang, G., Yuan, H., and Li, F., "Analysis of Creep-Fatigue Life Prediction Models for Nickel-based Super Alloys," *Comput. Mater. Sci.*, Vol. 57, 2012, pp. 80–88.

[9] Dowling, N. E., "Fatigue at Notches and the Local Strain and Fracture Mechanics Approaches," *Fracture Mechanics: Proceedings of the Eleventh National Symposium on Fracture Mechanics: Part I, ASTM STP 677*, C. W. Smith, Ed., Blacksburg, Va., June 12–14, 1978, ASTM International, West Conshohocken, PA, 1979, pp. 247–273.

[10] Benachour, N., Hadjoui, A., Benachour, M., and Benguediab, M., "Stress Ratio and Notch Effect on Fatigue Crack Initiation and Propagation in 2024 Al-Alloy," *Proc. World Acad. Sci. Eng. Technol.*, Vol. 79, 2011, pp. 566–569.

[11] Lazzarin, P., Tovo, R., and Meneghetti, G., "Fatigue Crack Initiation and Propagation Phases Near Notches in Metals with Low Notch Sensitivity," *Int. J. Fatigue*, Vol. 19(8–9), 1997, pp. 647–657.

[12] Furuya, Y. and Shimada, H., "Fatigue Crack Initiation from Notch Root (Local-Strain Damage Accumulation Process on Crack Initiation," *Eng. Fract. Mech.*, Vol. 23(6), 1986, pp. 983–989.

[13] Leidermark, D., Moverare, J., Simonsson, K., and Sjostrom, S., "A Combined Critical Plane and Critical Distance Approach for Predicting Fatigue Crack Initiation in Notched Single-Crystal Superalloy Components," *Int. J. Fatigue*, Vol. 33(10), 2011, pp. 1351–1359.

[14] Heckel, K. and Wanger, R., "Tensile Fatigue Behavior of C(T)-Specimens with Small Notch Root Radius," *Int. J. Fract.*, Vol. 11(1), 1975, pp. 135–140.

[15] Dowling, N. E. and Wilson, W. K., "Results of Elastic Analysis of Bluntly Notched Compact Specimens," *Eng. Fract. Mech.*, Vol. 20(3), 1984, pp. 569–572.

[16] Tanaka, K., Nakai, Y., and Kawashima, R., "Fracture Mechanics Approach to Fatigue Crack Initiation from Deep Notches," *Eng. Fract. Mech.*, Vol. 18(5), 1983, pp. 1011–1023.

[17] Creager, M. and Paris, P. C., "Elastic Field Equations for Blunt Cracks with Reference to Stress Corrosion Cracking," *Int. J. Fract. Mech.*, Vol. 3(4), 1967, pp. 247–252.

[18] ASTM E399-09$^{\varepsilon 2}$: Standard Test Methods for Linear-Elastic Plane-Strain Fracture Toughness, Kic, of Metallic Materials, *Annual Book of ASTM Standards*, ASTM International, West Conshohocken, PA.

[19] ASTM E647-08$^{\varepsilon 2}$: Standard Test Method for Measure of Fatigue Crack Growth Rates, *Annual Book of ASTM Standards*, ASTM International, West Conshohocken, PA, 2008.

[20] ASTM E1820-09$^{\varepsilon 1}$: Standard Test Method for Measurement of Fracture Toughness, *Annual Book of ASTM Standards*, ASTM International, West Conshohocken, PA, 2009.

[21] Keller, S. G., 2013, "Creep-Fatigue Crack Initiation and Propagation of a Notched Stainless Steel," Ph.D. dissertation, University of Central Florida, Orlando, FL.

[22] ASTM E8/E8M-09: Standard Test Method for Tension Testing of Metallic Materials, *Annual Book of ASTM Standards*, ASTM International, West Conshohocken, PA, 2009.

[23] ASTM E21-09: Standard Test Methods for Elevated Temperature Tension Tests of Metallic Materials, *Annual Book of ASTM Standards*, ASTM International, West Conshohocken, PA, 2009.

[24] Dowling, N. E. and Begley, J. A., "Fatigue Crack Growth During Gross Plasticity and the J-Integral," *Mechanics of Crack Growth, ASTM STP 590*, J. R. Rice and P. C. Paris, Eds., ASTM International, West Conshohocken, PA, 1976, pp. 82–103.

[25] Forman, R. G., Kearney, V. E., and Engle, R. M., "Numerical Analysis of Crack Propagation in Cyclic-Loaded Structures," *J. Basic Eng.*, Vol. 89(3), 1967, pp. 459–464.

[26] Elber, W., "The Significance of Fatigue Crack Closure," *Damage Tolerance in Aircraft Structures, ASTM STP 486*, P. S. Paris and R. J. Hebert, Eds., ASTM International, West Conshohocken, PA, 1971, pp. 230–242.

[27] Yamada, Y. and Newman, J. C., "Crack Closure under High Load-Ratio Conditions for Inconel-718 Near Threshold Behavior," *Eng. Fract. Mech.*, Vol. 76(2), 2009, pp. 209–220.

[28] *NASGRO User Manual*, v6.21. (2012). Southwest Research Institute, San Antonio, Texas.